Biochimica et Biophysica Acta 1808 (2011) 369–381

Contents lists available at ScienceDirect

Biochimica et Biophysica Acta

journal homepage: www.elsevier.com/locate/bbamem

Oligomeric structure of a cathelicidin antimicrobial peptide in dodecylphosphocholine micelle determined by NMR spectroscopy

Rathi Saravanan, Surajit Bhattacharjya *

School of Biological Sciences, Division of Structural and Computational Biology, Nanyang Technological University, Singapore 637551, Singapore

ARTICLE INFO

Article history:
Received 5 July 2010
Received in revised form 24 September 2010
Accepted 4 October 2010
Available online 8 October 2010

Keywords:
Antimicrobial peptide (AMP)
NMR
Oligomeric AMP
Antibiotic resistance

ABSTRACT

The broad spectrum of antibacterial activities of host defense cationic antimicrobial peptides (AMPs) arises from their ability to perturb membrane integrity of the microbes. The mechanisms are often thought to require assembly of AMPs on the membrane surface to form pores. However, three dimensional structures in the oligomeric form of AMPs in the context of lipid membranes are largely limited. Here, we demonstrate that a 22-residue antimicrobial peptide, termed VK22, derived from fowlicidin-1, a cathelicidin family of AMP from chicken oligomerizes into a predominantly tetrameric state in zwitterionic dodecylphosphocholine (DPC) micelles. An ensemble of NMR structures of VK22 determined in 200 mM perdeuterated DPC, from 755 NOE constrains including 19 inter-helical NOEs, had revealed an assembly of four helices arranged in anti-parallel fashion. Hydrogen bonds, $C^{\alpha}H—O=C$ types, and van der Waals interactions among the helical sub-units appear to be involved in the stabilization of the quaternary structures. The central region of the barrel shaped tetrameric bundle is non-polar with clusters of aromatic residues, whereas all the cationic residues are positioned at the termini. Paramagnetic spin labeled NMR experiments indicated that the tetrameric structure is embedded into micelles such that the non-polar region located inside the lipid acyl chains. Structure and micelle localization of a monomeric version, obtained from substitution of two Tyr residues with Ala, of the peptide is also compared. The mutated peptide VK22AA has been found be localized at the surface of the micelles. The tetrameric structure of VK22 delineates a small water pore that can be larger in the higher order oligomers. As these results provide structural insights, at atomic resolution, into the oligomeric states of a helical AMP in lipid environment, the structural details may be further utilized for the design of novel self-assembled membrane protein mimics.

1. Introduction

Host defense cationic AMPs are ubiquitously found in almost all forms of life [1–3]. AMPs being a part of the innate immune system constitute the first line of defense against invading bacteria, fungi and viruses in higher organisms including humans [1–3]. The cytolytic activities of many AMPs stem from their ability to lyse cell membranes of pathogens. Owing to the high content of positively charged and non-polar amino acid residues, AMPs readily integrate; often from unstructured states in aqueous solution, into cell membranes forming well defined amphipathic structures [1–3]. Interactions of AMPs with membranes can cause oligomerizations which are thought to be essential for their biological functions [4–6]. The mode of actions of AMPs have been described following three models (i) barrel stave, (ii) toroidal pore and (iii) carpet [2,7–10]. In the barrel stave and toroidal pore mechanisms, AMPs form self-assembled structures on the membrane surface necessary to stabilize pores or ion channels. In carpet mechanism, cell lysis may occur by aggregated AMPs utilizing a detergent-like feat [7–10]. In order to understand mechanisms of action, atomic-resolution structures of AMPs in oligomeric forms in lipid environments, either in micelles or in bilayers, are highly necessary. Although, lipid bilayers are closer mimic to the native cellular membranes, however atomic resolution structures of AMPs in such systems are difficult to obtain due to the large sizes [11,12]. Recently applications of solid state NMR have been proven successful to determine oligomerization and structural studies of AMPs in lipid bilayer [13–15]. On the other hand, atomic resolution structures, by use of solution NMR techniques, of AMPs are mostly determined in the context of small and fast tumbling detergent micelles e.g. negatively charged SDS and zwitterionic DPC [16–19] or dioctanoyl phosphatidylglycerol (D8PG) micelles [20]. A large number of studies suggest that these lipid micelles, SDS and DPC, predominantly favor monomeric structures of AMPs. However, oligomerization or dimerization for some AMPs have been detected in DPC micelles e.g. helical dimers of magainin analog MSI-78 [21], protegrin-1 [22], arenicins [23] and pleurocidin [24]. It is also noteworthy that DPC micelles are more frequently used, as compared to SDS micelles, as a model membrane mimic for structural studies of membrane proteins [25–27]. In some cases, DPC micelles not

* Corresponding author. Fax: +65 6791 3856.
E-mail address: surajit@ntu.edu.sg (S. Bhattacharjya).

0005-2736/$ – see front matter © 2010 Elsevier B.V. All rights reserved.
doi:10.1016/j.bbamem.2010.10.001

only preserve native structures of membrane proteins, but also help retain membrane enzymatic activities [27]. Recently, atomic resolution structures of some potent AMPs have been obtained in complex with lipopolysaccharide (LPS), the major component of outer membrane lipid of Gram negative bacteria, micelles [28,29].

Cathelicidins, originally identified in mammals, comprise a family of host defense antimicrobial proteins with a wide structural and sequence diversity [30–32]. These proteins are synthesized as a precursor containing a conserved cathelin domain at the N-terminus and an antimicrobial region at the C-terminus end. A large number of cathelicidin AMPs has helical amphipathicity including human cathelicidin LL37 [30–32]. The broad spectrum antibacterial activities of the cathelicidin AMPs like other potent AMPs stem from their efficient permeabilization and insertion into the bacterial membranes [30–32]. Three cathelicidin antimicrobial peptides are described in chicken [33–35]. These AMPs, termed fowlidicin-1, -2 and -3, are highly active against both Gram negative and Gram positive bacterial species including methicilin-resistant (MRSA) *Staphylococcus aureus* [33–35]. Notably, fowlicidins retain antimicrobial activities even in presence of salts [33]. By contrast, many AMPs including human cathelicidin LL37 are observed to be inactivated at high salt concentrations [30,31]. In addition, fowlicidins are also characterized by high affinity LPS or endotoxin neutralizations activities [33–35]. These functional attributes, including maintaining antimicrobial activities at high salt, of fowlicidins have been thought to be useful for treatment of cystic fibrosis and Crohn's disease, both of which are related with aberrant local expression or inactivation of antimicrobial peptides [33].

While carrying out NMR structural studies of 22-residue fowlicidin-1 or VK22, we observed oligomerization of this peptide in DPC micelles and also in LPS micelles. In this work, we demonstrate using pulse field gradient NMR, fluorescence, cross-linking experiments that VK22 oligomerizes predominantly into tetrameric states in DPC micelles. An ensemble of tetrameric structures of VK22 in perdeuterated DPC-d_{38} micelles is determined from NOE-driven distance and angular constraints using ^{1}H–^{1}H correlated two-dimensional NMR method [36]. The tetrameric structure of VK22, in DPC micelles, is characterized by a topology of antiparallel arrangement of four helices. Localization of VK22 helical structure in DPC micelles, probed by three different spin labeled compounds, namely Gd^{3+} chelated with 1,4,7,10-tetraazocyclododecane-tetraacetic acid (Gd^{3+}(DOTA)), 5-doxyl-stearic acid (5-DSA) and 16-doxyl-stearic acid (16-DSA), delineated that the central non-polar segment of the tetramer is largely embedded inside the hydrophobic core of the lipid micelles. By contrast, the positively charged patches at the termini of the helical bundle are either exposed to water or lay at the membrane/water interface. The interface of the tetrameric structure shows a small pore that in principle can cause permeation of water or ions. These results provide insights, at atomic resolution, into the assembly of a host defense cationic antimicrobial peptide and probable mechanisms of pore formation in lipid membranes by a helical AMP.

2. Materials and methods

2.1. Peptides and chemicals

All peptides, fowlicidin-1, VK22, VK22AA and fluorescein isothiocyanate (FITC) labeled VK22 (FITC-VK22) were synthesized commercially by GL Biochem (Shanghai, China) and further purified (≥96%) by a reverse-phase HPLC, Waters(tm)™, using a C_{18} column (300 Å pore size, 5 μm particle size) by a linear gradient of acetonitrile/water mixture. Molecular weight of the peptides, fowlicidin-1 (3141.70 dalton), VK22 (2601.25 dalton), VK22AA (2417.05 dalton) and FITC-VK22 (2989.88 dalton) was confirmed by mass spectrometry. DPC and deuterated compounds (DPC-d_{38}, D_2O, CD_3OH) were purchased from Avanti polar lipids (Alabama, USA) and Cambridge Isotope Laboratories, Inc. (Massachusetts, USA), respectively. Melittin, acrylamide, glutaraldehyde, paramagnetic lipids, 5-DSA, 16-DSA, were obtained from Sigma (St. Louis, MO, USA). Gd^{3+}(DOTA) was a gift from Dr. Konstantin Pervushin (Nanyang Technological University). 4,4-dimethyl-4-silapentane-1-sulfonic acid (DSS) was acquired from Cambridge Isotope Laboratories, Inc. (Massachusetts, USA). All other chemicals were of analytical grade.

2.2. NMR experiments

All NMR experiments were performed on a Bruker (Germany) DRX 600 MHz spectrometer, equipped with cryo-probe and pulse field gradients. NMR data processing and analysis were carried out using the programs Topspin (Bruker) and SPARKY, respectively. Samples for NMR studies were prepared by dissolving lyophilized VK22 or VK22AA powder (0.5 mM) into 200 mM perdeuterated DPC-d_{38} in 10 mM sodium phosphate buffer pH 4.8 containing 10% D_2O and DSS as internal standard. A series of 1-D NMR spectra of VK22 were acquired at various temperatures ranging from 298 K to 323 K. Spectral width was maintained at 12 ppm. All 2D experiments were recorded with 2K (t_2) × 400 (t_1) data points with a relaxation delay of 0.8 s for 72 (NOESY) and 24 (TOCSY) number of scans. 2-D NOESY (mixing time = 150 ms and 200 ms) and TOCSY (mixing time = 60 ms and 80 ms) experiments were performed for VK22 in 200 mM perdeuterated DPC-d_{38} in 10 mM phosphate buffer containing 10% D_2O, pH 4.5 either at 315 K (42 °C) or 323 K (50 °C). ^{13}C-^{1}H HSQC (at natural abundance) experiments for VK22 and VK22AA were done at 315 K, in 200 mM perdeuterated DPC-d_{38}, 10 mM sodium phosphate buffer in D_2O, pH 4.8. Spectral width was maintained at 12 (t_1) × 80 (t_2) ppm. A total of 2K (t_2) × 256 (t_1) data points were collected with a delay of 1 s with 56 transient. For the DPC micelle bound VK22AA (0.5 mM), 2-D NOESY (mixing time = 150 ms and 200 ms) and TOCSY (mixing time = 80 ms) experiments were performed in 200 mM perdeuterated DPC-d_{38} in 10 mM phosphate buffer containing 10% D_2O, pH 4.5 at 315 K.

Hydrogen–deuterium exchange studies of the DPC micelle bound VK22 and VK22AA were carried out by dissolving the lyophilized samples in 100% D_2O followed by collecting a series of two-dimensional ^{1}H-^{1}H NOESY spectra (mixing time = 150 ms) at time interval of 120 min for 7 h. The localization of VK22 in DPC micelles was studied using three spin labeled paramagnetic compounds 5-DSA, 16-DSA and Gd^{3+}(DOTA). Paramagnetic probes induced resonance perturbation experiments were performed by acquiring 2-D ^{1}H-^{1}H NOESY spectra in the absence and presence of 2 mM paramagnetic agents. The intensity of the intra-residue $C^{\alpha}H$-NH cross peaks was measured before and after the addition of the probes for 5-DSA and 16-DSA. For Gd^{3+}(DOTA) sidechain signals for cationic residues were considered.

Pulse field gradient (PFG) NMR method with PG-SLED pulse sequence was used to assess plausible oligomerization of VK22 and VK22AA peptides in DPC micelles [41]. Melittin, a bee venom toxin, was used as a reference molecule which is known to form a monomeric helical structure in DPC micelles [37]. Samples were prepared in 200 mM DPC-d_{38} containing 10 mM sodium phosphate buffer, pH 4.8. A series of 1-D proton NMR spectra with increased gradient strength from 2 to 95% were acquired at 315 K. The proton signal decay was then fitted to a single Gaussian expression: $I(g) = Ae^{-dg2}$, where I, g, d represent intensity of the signals, gradient strengths and decay rates, respectively.

2.3. NMR derived structure calculation

The 3-D structures of VK22 and VK22AA bound to DPC were calculated based on NOE derived distance constraints from 2D NOESY spectra and dihedral angle constrains obtained from TALOS [38] using the DYANA program, version 1.5 [39] as described previously [37]. On

the basis of cross-peak intensities NOEs were qualitatively categorized to strong, medium and weak and then translated to upper bound distance limits to 2.5, 3.5 and 5.5 Å, respectively. The lower bounds for all NOE restraints were set to 2.0 Å. Structure calculations were carried out in stepwise fashion. Initially, an ensemble of monomeric helical structures of VK22 were derived using sequential (i to $i+1$) and diagnostic medium range NOEs e.g. $C^{\alpha}H$ to NH, (i to $i+2$, $i+3$ and $i+4$), $C^{\alpha}H/C^{\beta}H$ (i to $i+3$). Along with the helical NOEs used for monomeric structure, the long-range NOEs, from residues N- and C-termini, were then further utilized to generate an antiparallel dimer. While structure calculation of the dimer, two chains (A and B) of VK22 were connected by a Gly-linker. In this round of structure calculation, NOEs showing a large violation in distance constraints (>0.9 Å) were filtered out. These NOEs were subsequently utilized to determine the tetrameric assembly whereby four chains (A, B, C and D) of VK22 were linked by three Gly-linkers. The final ensemble of tetrameric structures of VK22 was of good quality defined by low RMSD and low violation of distance and dihedral angle constraints.

2.4. Fluorescence studies

Fluorescence experiments were carried out in Cary Eclipse fluorescence spectrophotometer (Varian, Inc., Australia) equipped with a dual monochromators. All measurements were performed using 0.1 cm path length cuvette and a slit width of 5 nm. Intrinsic tryptophan fluorescence spectra of free peptide was recorded using 5 μM VK22 in 10 mM sodium phosphate buffer pH 6.8 or in complex with DPC micelles (1.4 mM) in the same buffer. An excitation wavelength of 280 nm was used and the emission was monitored between 300 and 400 nm. Fluorescence quenching experiments for free and micelle bound peptide were recorded by stepwise addition of (0.02–0.2 M) of acrylamide either into the peptide or peptide-DPC complex solutions. Quenching of fluorescence intensity at emission maxima for corresponding free and micelle bound forms were noted and results were analyzed using Stern–Volmer quenching equation $F_o/F = 1 + K_{sv}[Q]$, where F_o and F are the fluorescence intensity at emission maxima in the absence and presence of quencher, respectively, K_{sv} is the Stern–Volmer quenching constant and [Q] is the molar concentration of acrylamide. Quenching of fluorescein isothiocyanate (FITC) conjugated VK22 upon association with DPC lipids was acquired by titrating 5 μM FITC-VK22 with increasing concentration of DPC. FITC conjugated peptide was excited at 480 nm and emission was monitored from 500 to 600 nm. All the experiments were carried out in 10 mM sodium phosphate buffer, pH 6.8.

2.5. Antibacterial assay

Antibacterial activity against Gram negative bacteria *Escherichia coli*, *Pseudomonas aeruginosa* (ATCC 27853), Gram positive bacteria *S. aureus* (ATCC 25923) and *Bacillus subtilis* were analyzed for the 26-residue fowlicidin-1, VK22 and VK22AA. Mid-log phase bacterial cells obtained from an overnight culture were washed thrice with 10 mM phosphate buffer containing 150 mM NaCl (pH 7.4), and resuspended to an optical density of 0.2 at 600 nm. Equal volumes (50 μl) of the respective bacterial cultures were incubated with serially diluted peptides in a 96 well micro titer plate, incubated at 37 °C for 3 h and streaked on Muller Hilton agar plates. After overnight incubation at 37 °C, the lowest peptide concentration yielding bacterial growth inhibition was noted as the MIC value for each of the corresponding peptides.

2.6. Cross linking in DPC micelles

Either VK22 or VK2AA at 100 μM concentration in the presence of DPC micelles (10 mM) in 10 mM sodium phosphate buffer were cross-linked with increasing concentration of glutaraldehyde (2.5%, 5%, 7.5% and 10%) or in the absence of glutaraldehyde in dark at 37 °C for overnight. Equal volume (10 μl) of sodium dodecyl sulfate polyacrylamide (SDS-PAGE) gel electrophoresis loading dye containing β-mercaptoethanol was added to the cross-linked samples, boiled for 10 min and analyzed by 17% tris-tricine SDS-PAGE gel.

Table 1
Antibacterial activity of Fowlicidin-1, VK22 and VK22AA.

Peptide	MIC (μM)[a]			
	E. coli	*P. aeruginosa*	*S. aureus*	*B. subtilis*
Fowlicidin-1	1.6	1.6	1.6	1.6
VK22	1.6	1.6	1.6	1.6
VK22AA	12.5	6.2	3.1	6.2

[a] MIC, minimum inhibitory concentration.

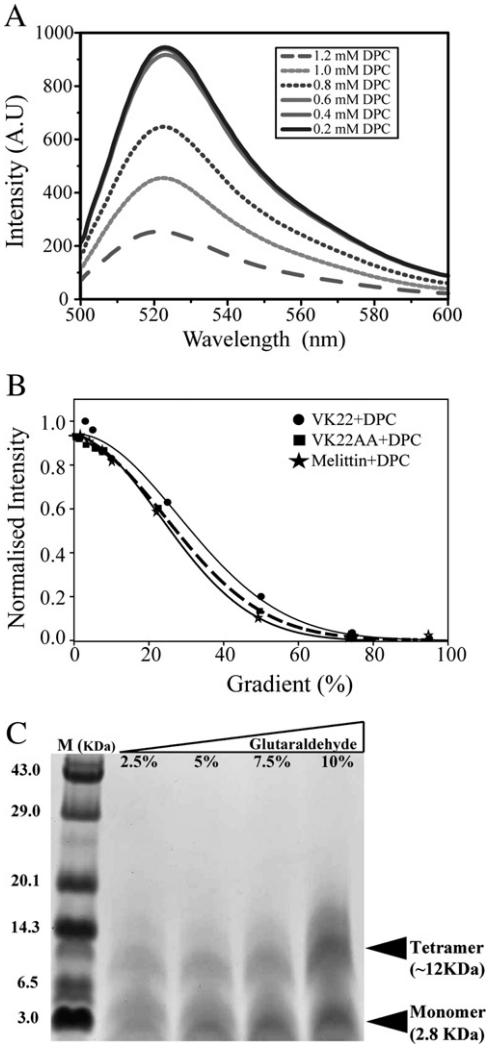

Fig. 1. Oligomerization of VK22 in DPC micelles: (A) Quenching of FITC fluorescence intensity of FITC-conjugated VK22 as a function of concentrations of DPC, indicating self association of peptide in the lipid micelles. Experiments were carried out in 10 mM sodium phosphate buffer, pH 6.8. Samples were excited at 480 nm and FITC fluorescence emission was monitored from 500 to 600 nm wavelength. (B) Plot showing normalized reduction in NMR signal intensity with increasing strength of gradient for VK22, VK22AA and melittin in 200 mM DPC-d_{38}. (C) SDS-PAGE gel showing oligomerization of VK22 at various concentrations of glutaraldehyde namely 2.5% (lane 2, from left), 5% (lane 3), 7.5% (lane 4) and 10% (lane 5). The protein bands at the first lane (marked as M) correspond to molecular weight references. As can be seen, a protein band for VK22 corresponding to molecular weight ~12 kDa (tetramer) is present upon cross-linking with glutaraldehyde. At high concentration of cross-linker (10%), a population for higher order oligomer (MW ~19 kDa) is also detectable (lane 5, from left).

3. Results

3.1. Oligomerization of 22-residue fowlicidin-1 or VK22 in DPC micelles

The size of mature antibacterial domain of cathelicidin derived AMPs are putatively assigned based on proteolytic cleavage sites [30–32]. The full-length antimicrobial domain of fowlicidin-1 (RVKRVWPLVIRTVIAGYNLYRAIKKK) has been predicted, based on an elastase cleavage site, to be of 26-residue, [33]; however a deletion of four residues at the N-terminus, yielding a 22-residue fragment (VWPLVIRTVIAGYNLYRAIKKK), does not affect the antibacterial activities and membrane disruption by the peptide (Table 1) [34]. Due to favorable spectral behavior in complex with DPC micelles required for NMR studies the 22-residue fowlicidin-1 or VK22 has been utilized here. The oligomerizations of VK22 in DPC micelles have been probed from various experiments. We have assessed changes of fluorescence intensity of fluorescein isothiocyanate (FITC) labeled VK22 (FITC-VK22) in the context of DPC. The fluorescence intensity of FITC would be quenched while FITC-labeled molecules undergo self-associations [40]. As can be seen, the fluorescence intensity of FITC-

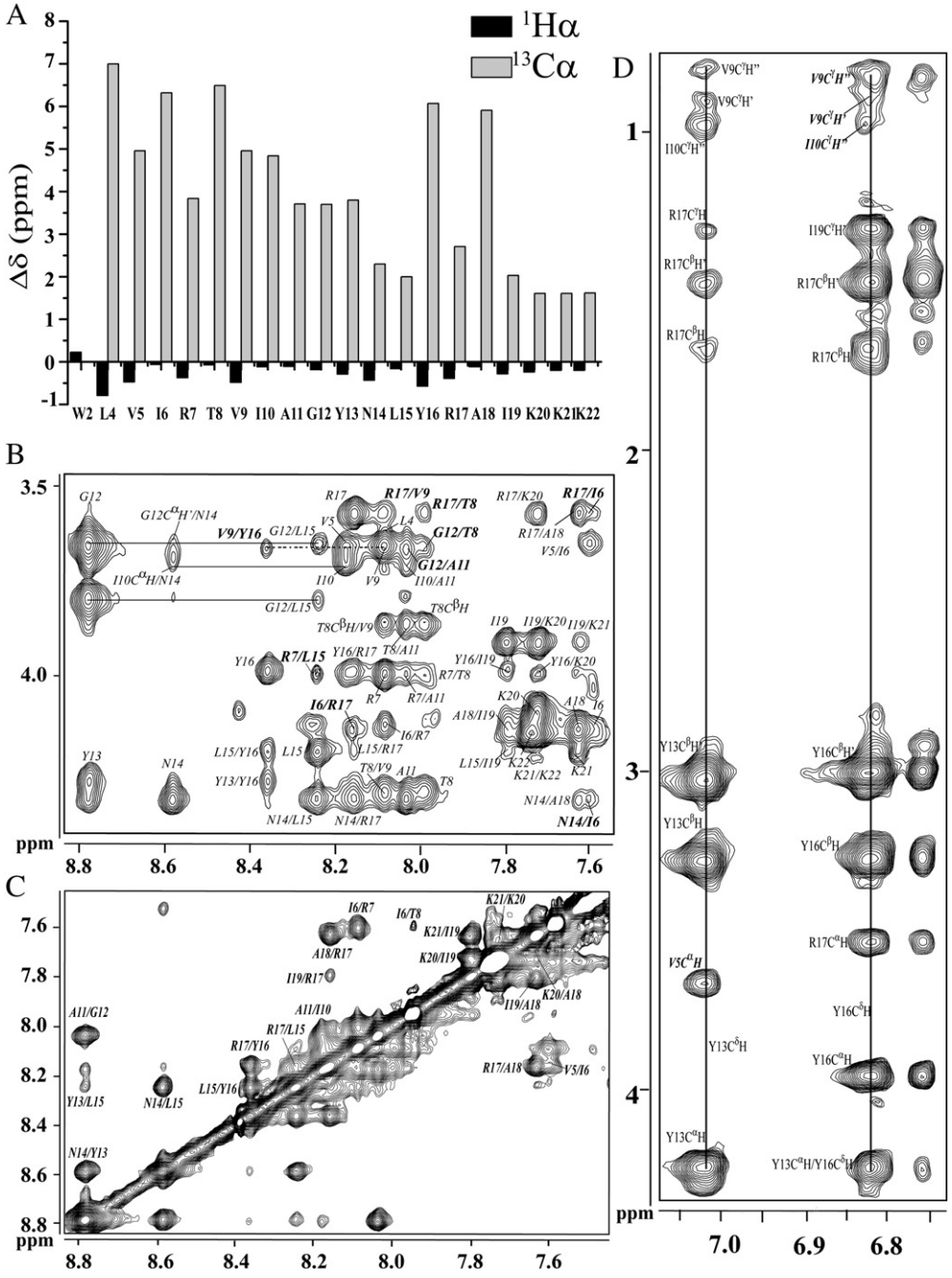

Fig. 2. NMR studies of VK22 in DPC micelles: (A) Chemical shift deviation of the $C^{\alpha}H$ protons and $^{13}C^{\alpha}$ resonances of VK22 from random coil values in complex with DPC micelles. (B) Finger print region of the two dimensional $^1H-^1H$ NOESY spectrum of VK22 in 200 mM DPC-d_{38} showing sequential, medium range and long range NOE connectivities. Long-range NOEs are marked as bold and italicized. (C) A section of the two dimensional $^1H-^1H$ NOESY spectrum of VK22 bound to DPC micelles delineating sequential NH/NH NOEs. (D) A selected region of two dimensional $^1H-^1H$ NOESY spectrum, obtained in D_2O, of VK22 in 200 mM DPC-d_{38} representing long-range NOEs among aromatic ring proton resonances of residues Tyr13, Tyr16 with aliphatic sidechain proton resonances. Long-range NOEs are marked as bold and italicized.

VK22 shows significant quenching with increasing concentrations of DPC, indicating oligomerization of VK22 in lipid micelles (Fig. 1A). Pulse field gradient (PFG) based diffusion NMR experiments are often been used to detect oligomerizations of proteins, peptides in aqueous solution and also in lipid membranes [41]. We compare diffusion behavior of the native VK22 peptide, a mutated version of VK22 or VK22AA, containing two replacements at Y13A and Y16A and 26-residue melittin, as a reference molecule. The native VK22 shows retarded diffusion in DPC micelles as compared to the mutated peptide and melittin (Fig. 1B), further supporting oligomerization of VK22 in DPC micelles. NMR data suggest that the mutated VK22AA is monomeric in DPC micelles (*vide infra*). In the glutaraldehyde mediated cross-linking experiments, VK22 demonstrated to form predominantly tetrameric states in complex with DPC micelles (Fig. 1C, panel E). There is a prominent band in the SDS-PAGE gel corresponding to molecular weight of ~12 kDa arises upon incubation of VK22/DPC with cross-linker (Fig. 1C). The intensity of the gel band augmented with the concomitant increase in concentrations of glutaraldehyde (Fig. 1C). At higher concentrations of glutaraldehyde, cross-linked species belonging to larger molecular weight, 15–20 kDa, are also be seen albeit with lesser populations (Fig. 1C). By contrast, DPC-bound VK2AA did not show cross-linked products and remains largely monomeric (Supplementary Figure S1). Both peptides, VK22 or VK22AA, appear to migrate on the SDS-PAGE gels as monomeric species without cross-linker (Supplementary Figure S1). The absence of detectable oligomerization of VK22 in the SDS-PAGE gels, without glutaraldehyde treatment, may indicate that the non-covalent association among peptides could be disrupted by SDS detergent. Taken together, these data suggest that VK22 forms a self-assembled tetrameric state in DPC lipid micelles.

3.2. NMR Studies of VK22 in DPC Micelles

A molecular weight of ~22 kDa is expected for the tetrameric VK22/DPC complex, considering a molecular mass of 12 kDa for the DPC micelle [11]. As a result of high molecular weight of the micelle/peptide complex, good quality NMR spectra can only be obtained at higher temperatures e.g. 42 °C or 50 °C. VK22 yielded well-dispersed high-quality NOESY spectra at 42 °C (Fig. 2). NOESY spectra obtained at 50 °C showed more overlapping resonances as compared to that of 42 °C. Therefore, we have chosen 42 °C as preferred NMR condition for further structural analyses. In the absence of lipid micelles, VK22 assumes random conformations in aqueous solution as judged from limited number of NOEs (Supplementary Figure S2).

Sequence-specific resonance assignments of DPC-bound VK22 are achieved from 2D NOESY and TOCSY spectra [36]. The deviation of $^{13}C^{\alpha}$ and $C^{\alpha}H$ chemical shifts from random coil value is an indicator of secondary structures of proteins and peptides [42]. In helical structures, $^{13}C^{\alpha}$ chemical shift experiences a downfield shift or positive deviation whereas $C^{\alpha}H$ chemical shift shows an opposite trend [42]. The $^{13}C^{\alpha}$ resonances (obtained from natural abundance ^{13}C–^{1}H correlation spectra) of residues L4-K22 of VK22 show a marked positive deviation from random coil chemical shifts (Fig. 2A). The $C^{\alpha}H$ chemical shifts of these residues are also further characterized by an upfield shift or negative deviation from random coil values (Fig. 2A). Thus, based on these chemical shift deviations, VK22, for residues L4-K22, appears to adopt helical conformation in the DPC micelles. Analyses of ^{1}H–^{1}H NOESY spectra of DPC-bound VK22 reveal diagnostic medium range NOEs, $C^{\alpha}H$ to NH (i to i + 3, i + 4), $C^{\alpha}H$ to $C^{\beta}H$ (i to i + 3)) and NH/NH (i to i + 1 and i + 2) NOEs encompassing residues L4 to K22, supporting helical structure in DPC micelles (Fig. 2B and C and Fig. 3). The first three residues, V-W-P, at the N-terminal region of VK22 do not show any medium range NOEs, indicating an extended conformation for this segment. Further, the $C^{\alpha}H$ chemical shift of W2 has been found to have a positive deviation, implying non-helical conformation (Fig. 2A). However,

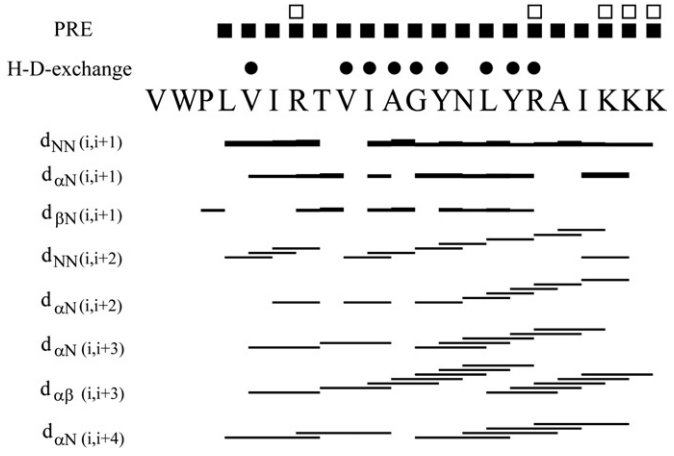

Fig. 3. NOE summary: Bar diagram summarizing sequential and medium range NOE connectivities of VK22 in DPC micelles. Residues of VK22 showing slow exchange amide proton against solvent D_2O in DPC micelles are indicated by filled circle at the top of the sequence. Residues of VK22 showing resonance perturbation in 5-DSA and 16-DSA paramagnetic probes and for cationic residues by Gd^{3+}(DOTA) are marked by filled square and open square, respectively.

intrinsic Trp fluorescence studies demonstrate that the N-terminal region is located inside lipid micelles (*vide infra*). As would be expected, analyses of NOESY spectra of VK22 in DPC micelles demonstrated several long-range NOE contacts, from residues at the N-terminus to the residues at the C-terminus of it e.g. R7C^{α}H/L15NH, V9C^{α}H/Y16NH, I6C^{α}H/R17NH, supporting anti-parallel oligomerization of the helical structure (Fig. 2B). The ring proton resonances of residues Y13 and Y16 show a number of long-range NOE contacts with the aliphatic sidechain of residues V9 and I10 (Fig. 2D). In addition, we have also found few sequential/medium range NOEs e.g. Nα types (G12C^{α}H/A11NH and G12C^{α}H/T8NH), which are otherwise not compatible to monomeric helical conformations (Fig. 2B). These NOEs are therefore plausibly arising as a result of close proximity of the helical subunits. Table 2 summarizes all the nineteen inter-helical NOEs, including backbone/backbone, sidechain/backbone and sidechain/sidechain, used for the structure determination of the tetrameric VK22 (Supplementary Figure S3).

Table 2
Summary of key inter-helical NOEs used to define the tetrameric structure of VK22 in DPC micelle[a].

Inter-helical NOEs	
I6HN	***N14C^{α}H***
R7C^{α}H	***L15HN***
I6HN	***R17C^{α}H***
V9HN	***R17C^{α}H***
V9C^{α}H	***Y16HN***
G12C^{α}Hs	***A11HN***
G12C^{α}Hs	***T8HN***
T8C^{α}H	***R17HN***
V5C^{α}H	***Y13C^{δ}H***
V9$C^{\gamma}H_1$	***Y16C^{δ}Hs***
V9$C^{\gamma}H_2$	***Y16C^{δ}Hs***
I10C^{γ}Hs	***Y16C^{δ}Hs***
V9C^{γ}Hs	G12C^{α}Hs
V5C^{β}H	I19C^{γ}Hs
V5C^{γ}Hs	I19C^{δ}Hs
T8C^{γ}Hs	L15C^{γ}H
T8C^{γ}Hs	L15C^{β}Hs
V5C^{γ}Hs	I19C^{γ}Hs
V9C^{γ}Hs	L15C^{β}Hs

[a] NOEs those are indicated in the Fig. 2 (panels B and D) are italicized bold, other NOEs are identified in Fig. S3.

3.3. Solution structure of VK22 in DPC micelles

NOESY spectra of VK22 in DPC micelles delineated NOE contacts among residues situated at the N-terminus and C-terminus; qualitatively indicating an anti-parallel arrangement of the helices (Fig. 2). All of these long-range NOEs were used to determine an anti-parallel dimeric structure of VK22. However, several inter-helical NOEs show violation of distance constraints >0.9 (experimental section) and could not be satisfied into a dimeric structure (Fig. 4A). This observation implies that helices of VK22 may be associating through two distinct interfaces forming the tetramer, whereby in the dimeric configuration one of these interfaces remains close as marked as H1/H2, while other interface termed as H3/H4 will stay far (Fig. 4A). A tetrameric structure i.e. dimer of dimer, demonstrated to satisfy all of the observed inter-helical NOEs (Table 2, Fig. 2). It may be noted that due to the overlapping resonances seven (out of nineteen) NOE derived distance constraints involving aliphatic sidechains (Table 2, Supplementary Figure S3) were used at the later stage of structure calculation upon observing proximity of these sidechains in initially generated conformers.

Fig. 4 shows superposition of an ensemble of twenty lowest energy tetrameric structures of VK22 in complex with DPC micelles (Fig. 4B). The backbone atoms (C^{α}, C′ and N) and the heavy atoms of the tetrameric structural ensemble of the VK22 (residues V1-K22), show RMSDs of 1.9 and 2.6 , respectively (Table 3). The individual helical structure of VK22 spans from residues L4-K21, while the first three residues, V–P–W, at the N-terminus remain largely extended. Four helices of the tetramer are represented as helix A (yellow), helix B (pink), helix C (green) and helix D (gray) (Fig. 4C and 4D). Helix A and helix B forms an antiparallel dimer as of helices C and D (Fig. 4C and 4D). Interestingly, the antiparallel arrangement of the four helices of VK22 places all of the positively charged sidechains e.g. R7, R17, K20, K21 and K22 at the two ends of the quaternary structure (Fig. 4E). Essentially, the barrel shaped tetrameric structure of VK22 contains large positively charged surfaces at the termini and a non-polar region at the middle (Fig. 4E).

Table 3
Summary of structural statistics for the twenty lowest energy tetrameric structures of DPC micelle bound VK22.

Distance restraints	
Intraresidue ($i–j=0$)	236 (59×4)
Sequential ($\|i–j\|=1$)	216 (54×4)
Medium-range ($2\leq\|i–j\|\leq4$)	284 (71×4)
Inter-helical NOE	19
Total NOE constraints	755
Angular restraints	
ϕ	80 (20×4)
ψ	80 (20×4)
Distance restraints violations	
No. of violations	12
Average NOE violation (Å)	<0.34
Maximum NOE violation (Å)	<0.49
Average target function values	12.72 (13.52–11.03)
Deviation from mean structure	
Backbone atoms (N, C^{α}, C′) (Å)	1.9±0.4
Heavy atoms (Å)	2.6±0.3
Ramachandran plot analysis	
Residues in the most favorable region	96.4%
Residues additionally allowed region	4.6%
Residues in the generously allowed region	0%
Residues in the disallowed region	0%

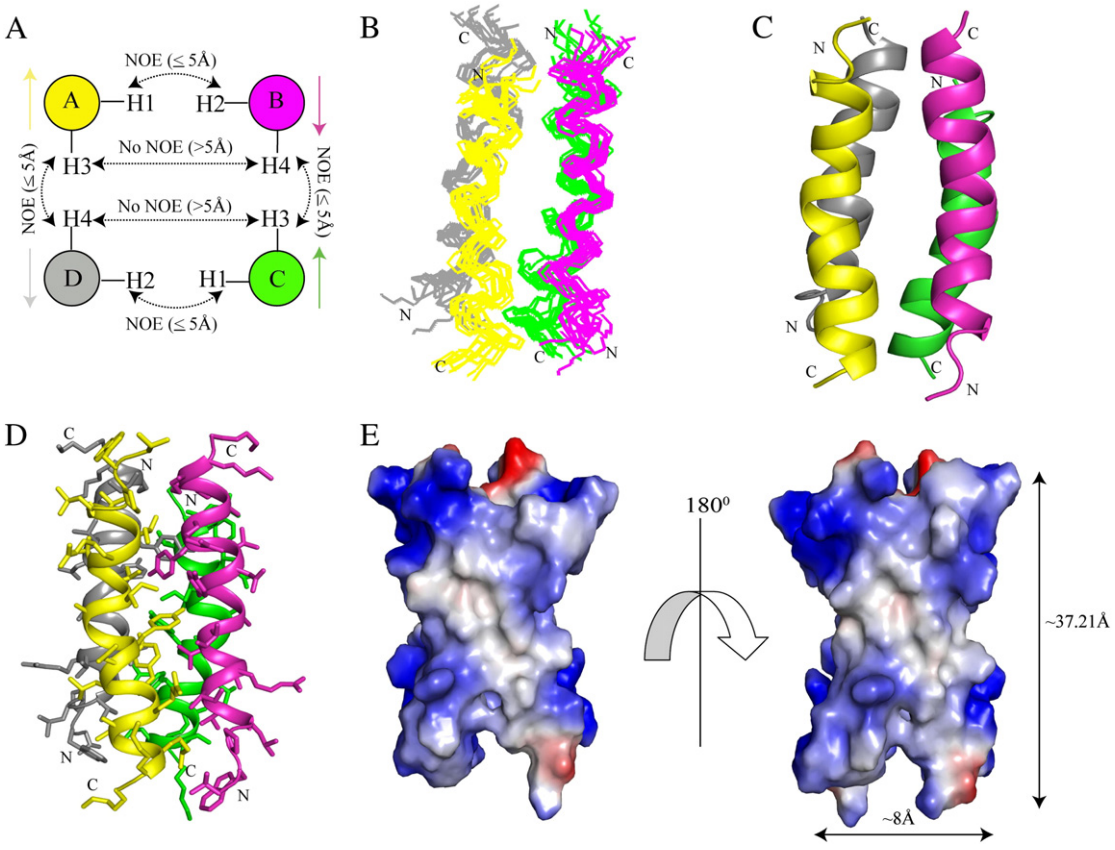

Fig. 4. 3-D structure of the tetramer. (A) Schematic representation of inter-helical NOE contacts among the four different subunits (A, B, C and D) of tetramer, viewing down the axis of the helix, in an antiparallel arrangement that can satisfy two interfaces of the tetramer. (B) Superposition of backbone atoms of the twenty lowest energy structures of VK22 tetramer in DPC micelles. Ribbon representation of a selected tetrameric structure, showing backbone fold (C) and sidechain disposition (D). (E) Electrostatic surface of the tetrameric structure of VK22 in DPC micelles. The dimension of the tetrameric structure has also been shown.

The quaternary structure of VK22 in DPC micelles appear to be stabilized by potential inter-helical hydrogen bonds. Notably, there are C^{α}—H—O type hydrogen bonds at the helical interfaces e.g. involving $C^{\alpha}H_s$ of Gly12 and C O of Thr8 between helix A (helix B) and helix D (helix C) (Fig. 5A). The sidechain OH proton of Thr8 is also in close proximity to the C O of Gly12 implicating backbone/sidechain hydrogen bonding (Fig. 5A). These hydrogen bonds, especially those involving residues Gly/Ala, are abundantly found in the trans-membrane (TM) helices and considered to be important for oligomerization of TM helices in membranes [43–45]. Indeed, T(8)-XXX-G(12) motif present in fowlicidin-1 had been identified as one of the typical sequence patterns for oligomerization of TM helices of membrane proteins [44,45]. In addition to these polar interactions, the antiparallel helices demonstrate van der Waals packing among non-polar residues (Fig. 5B). The helical interfaces between helix A and helix B or helix D and helix C are formed by sidechain/sidechain packing among aromatic residue Y13 and part of alkyl sidechain of R17 from one subunit with non-polar residues I6 and V9 from other helical subunit (Fig. 5B). Further, the oligomerization of VK22 peptide in DPC micelles has rendered formation of two aromatic clusters consisted of eight Tyr residues (Fig. 5C). Both Tyr residues, Y13 and Y16, from all the four helical subunits of the tetrameric structure of VK22 are found to have mutual interactions forming a defined non-polar core (Fig. 5C). A set of non-polar residues, L4, V5, I10, A11, L15, A18 and I19, are exposed outside the tetrameric structure of VK22 peptide in DPC micelles (Fig. 5D). The hydrophobic exposed surface area of the VK22 tetramer has been estimated to be ~4800 $Å^2$. This non-polar surface may plausibly interact with acyl chains of the lipid micelles. It is noteworthy that the sidechain of residue R7 from one helix is complemented by potential hydrogen bonds with the sidechain of residue N14 from the adjacent helix, indicating polar interactions at the outer surface of the tetramer (Fig. 5E).

3.4. Structure and oligomerization of VK22AA peptide

In order to understand the probable significance of the clustering of aromatic residues in the oligomerization and activity of VK22, a mutated peptide containing Ala replacements, Tyr13 to Ala and Tyr16 to Ala, was made. The analog peptide showed lower antibacterial activities as compared to the native VK22 (Table 1). PFG-NMR and cross-linking studies show that VK22AA peptide does not self associate in DPC micelles (Fig. 1B, Supplementary Figure S1). NMR analyses demonstrate VK22AA assume a monomeric helical structure in DPC micelles (Fig. 6). The positive deviation of $^{13}C^{\alpha}$ and the negative deviation of $C^{\alpha}H$ chemical shifts from random coil support helical conformations of the peptide in DPC micelles (Fig. 6A). Fig. 6B shows the differences in chemical shift deviations, for all but three N-terminal residues and residues at position 13 and 16, for $^{13}C^{\alpha}$ and $C^{\alpha}H$ nuclei, between VK22 and VK22AA peptide. The $^{13}C^{\alpha}$ chemical shifts appear to be largely affected between the tetrameric VK22 and

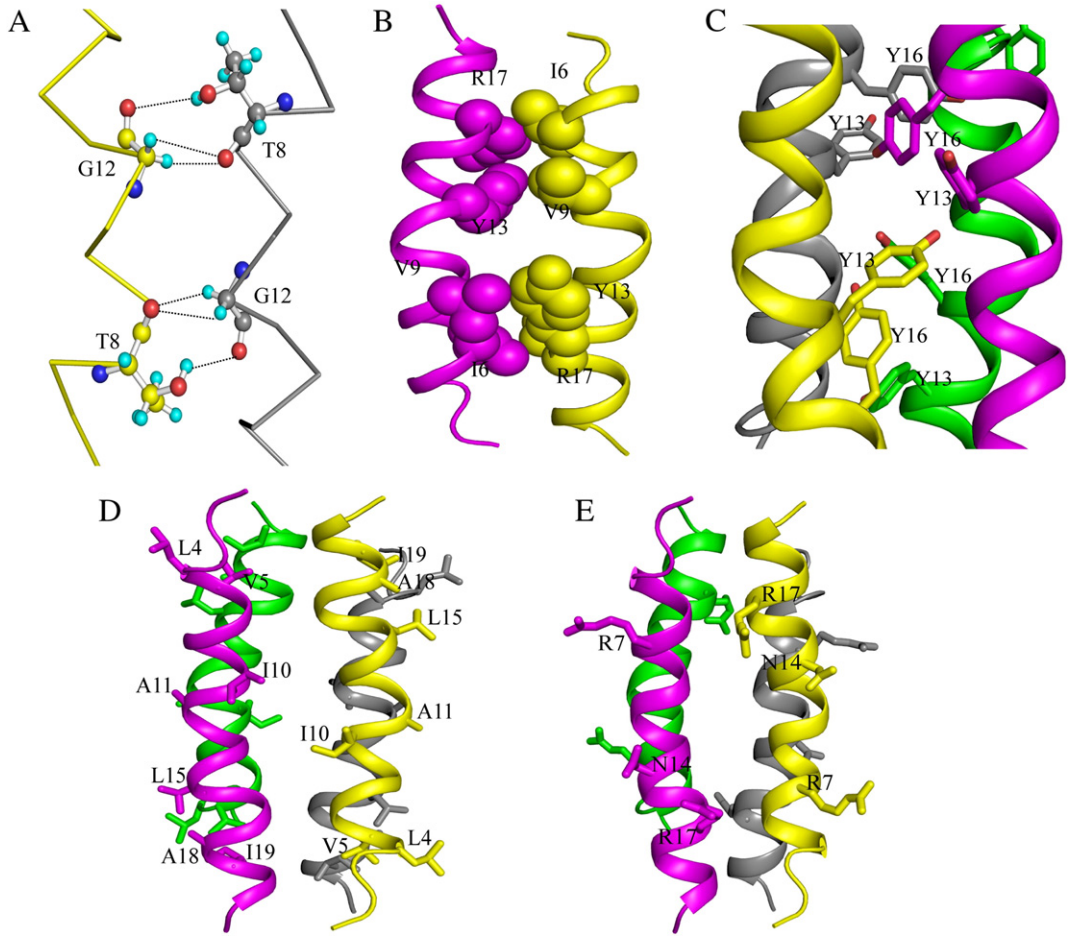

Fig. 5. Inter-helical interactions in the tetramer. (A) Potential inter-helical $C^{\alpha}H$—O C type hydrogen bonds between $C^{\alpha}H$ protons of residue G12 (helix D) with carbonyl oxygen of residue T8 (helix A). The sidechain hydroxyl group of T8 in close proximity with carbonyl oxygen of G12 may form additional hydrogen bonds. These potential hydrogen bonds are also present between helix B and helix C due to the symmetry. (B) Inter-helical van der Waals packing interactions among the non-polar sidechains of amino acid residues, V9, I6 Y13, and R17 of VK22 between helix A (or helix C) and helix B (or helix D). (C) Dispositions of the aromatic residues in the tetrameric structure of VK22 in DPC micelles showing clustering of Tyr residues at the helical interface. (D) Exposed hydrophobic residues, L4, V5, I10, A11, L15, A18 and I19 of VK22 tetramer. These residues are amenable for interactions with the fatty acyl chain of lipid micelles. (E) Residues R7 and N14 are exposed and in close proximity in the tetrameric structure of VK22. The sidechains of R7 and N14 may be engaged in polar interactions between the helical subunits.

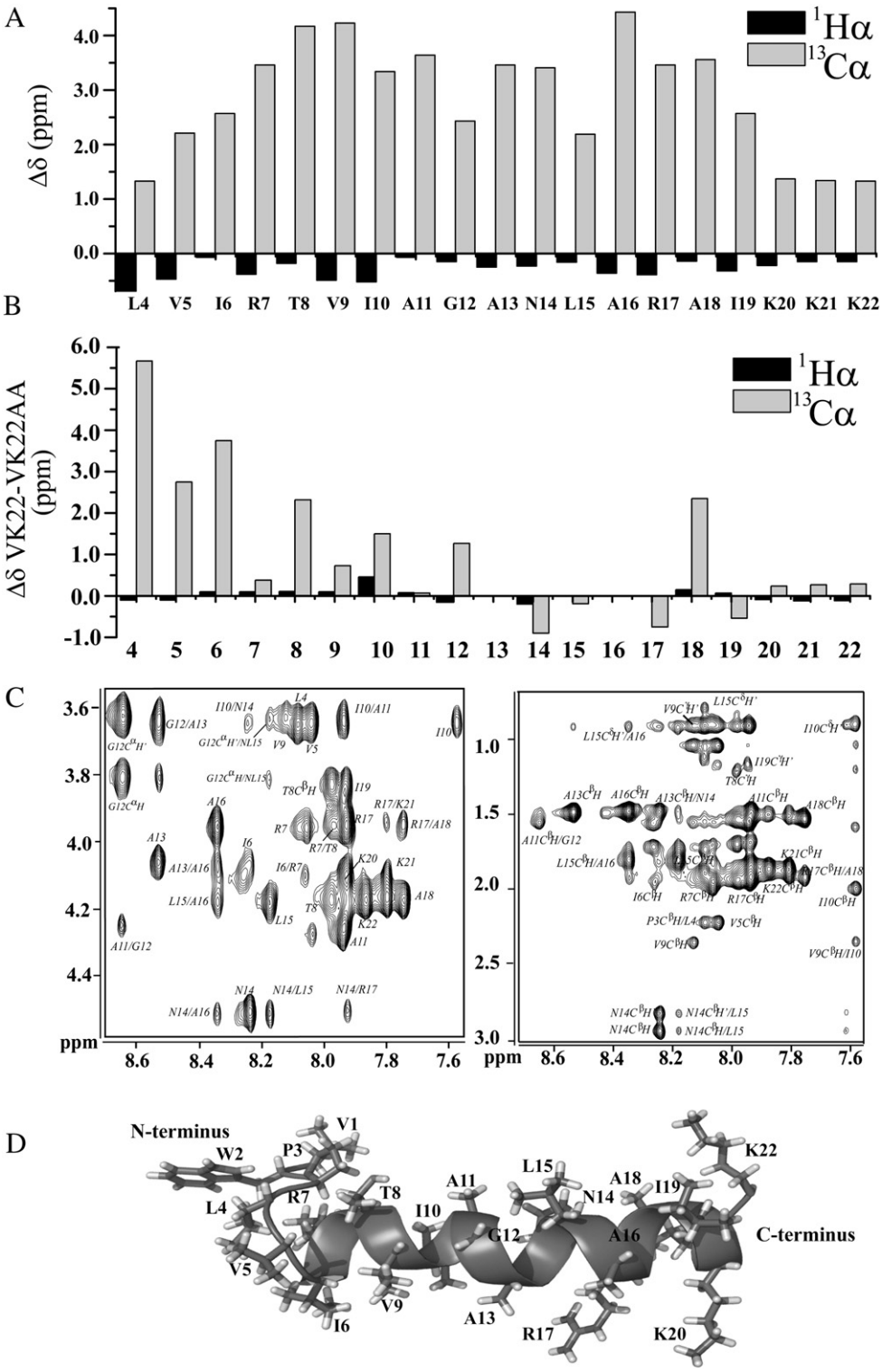

Fig. 6. NMR studies of VK22AA peptide in DPC micelles. (A) Chemical shift deviation of the $C^{\alpha}H$ protons and $^{13}C^{\alpha}$ resonances of VK22AA from random coil values in complex with DPC micelles. (B) Differences in the chemical shift deviation values for $^{13}C^{\alpha}$ and $C^{\alpha}H$ between tetrameric VK22 and monomeric VK22AA peptides. (C) ^{1}H–^{1}H 2D NOESY spectra of VK22AA in DPC micelles for the finger print region (NH/$C^{\alpha}H$) (left panel) and amide proton (NH) to aliphatic sidechain resonances (right panel), showing sequential and intra-residue NOE connectivities. (D) Ribbon representation of a representative monomeric helical structure of the VK22AA peptide derived from structure calculation. The sidechain of the amino acids is represented as sticks.

monomeric VK22AA peptide (Fig. 6B). The two-dimensional NOESY spectra of VK22AA in DPC micelles display only sequential and medium range NOEs akin to monomeric helical conformation (Fig. 6C). The paucity of long-range NOEs in the NOESY spectra of VK22AA indicates lack of any detectable oligomerizations. The solution structure of VK22AA in DPC micelles is characterized by a presence of a loop, for residues V1-L4, at the N-terminus followed by a helix encompassing residues V5-K22 (Fig. 6D). Backbone amide proton exchange with solvent D_2O demonstrated that VK22AA is much less protected against exchange as compared to VK22, indicating a plausible surface localization of the mutated peptide (Supplementary Figure S4). These results further underscore the

likely significance of aromatic interactions among these Tyr residues in stabilizing quaternary association of VK22 in lipid micelles.

3.5. Localization of the tetrameric structure of VK22 in DPC micelles

The depth of micelle insertion of the DPC-bound structure of VK22 has been delineated by NMR resonance perturbations induced by three paramagnetic probes 5-DSA, 16-DSA and Gd^{3+}(DOTA) [46]. The 5-DSA and 16-DSA will enhance relaxation or line broadening of the NMR resonances of the amino acid residues located inside lipid micelles, whereas Gd^{3+}(DOTA) is effective against water exposed signals [46]. Specifically, AMPs located at the micelle surface with a parallel orientation would be experiencing relaxation enhancement by 5-DSA and Gd^{3+}(DOTA), with a limited perturbation from 16-DSA [11,47,48]. Here, almost all the backbone HN/C^{α}H correlations of VK22 were found to be affected both by 5-DSA and 16-DSA (Fig. 7A). A ratio of 1, remaining signal amplitude of 5-DSA/16-DSA, in the Fig. 7A indicates that equal perturbation of the resonances by spin labeled probes, whereas a lower ratio of <1 refers to more perturbation by 5-DSA. A ratio of >0.70 or equal to 1 can be seen for all but two residues L4 and I6. Interestingly, the resonance perturbation by water soluble quencher Gd^{3+}(DOTA) was highly limited. Only the sidechain resonances of the terminal cationic residues were affected by addition of Gd^{3+}(DOTA) (Fig. 7B). Solvent exposure of the tetrameric structure of VK22 was also examined by the backbone amide proton (H—D) exchange studies. Several hydrophobic residues, V5, V9-R17, including those are located at the central region of the tetramer showed strong protection against exchange with solvent D_2O (Fig. 3, Supplementary Figure S4). These data clearly demonstrate that the oligomeric structure of VK22 is deeply embedded in the DPC micelles with a very limited exposure to the aqueous solutions. The pattern of resonance perturbations by the relaxation probes and a limited H/D

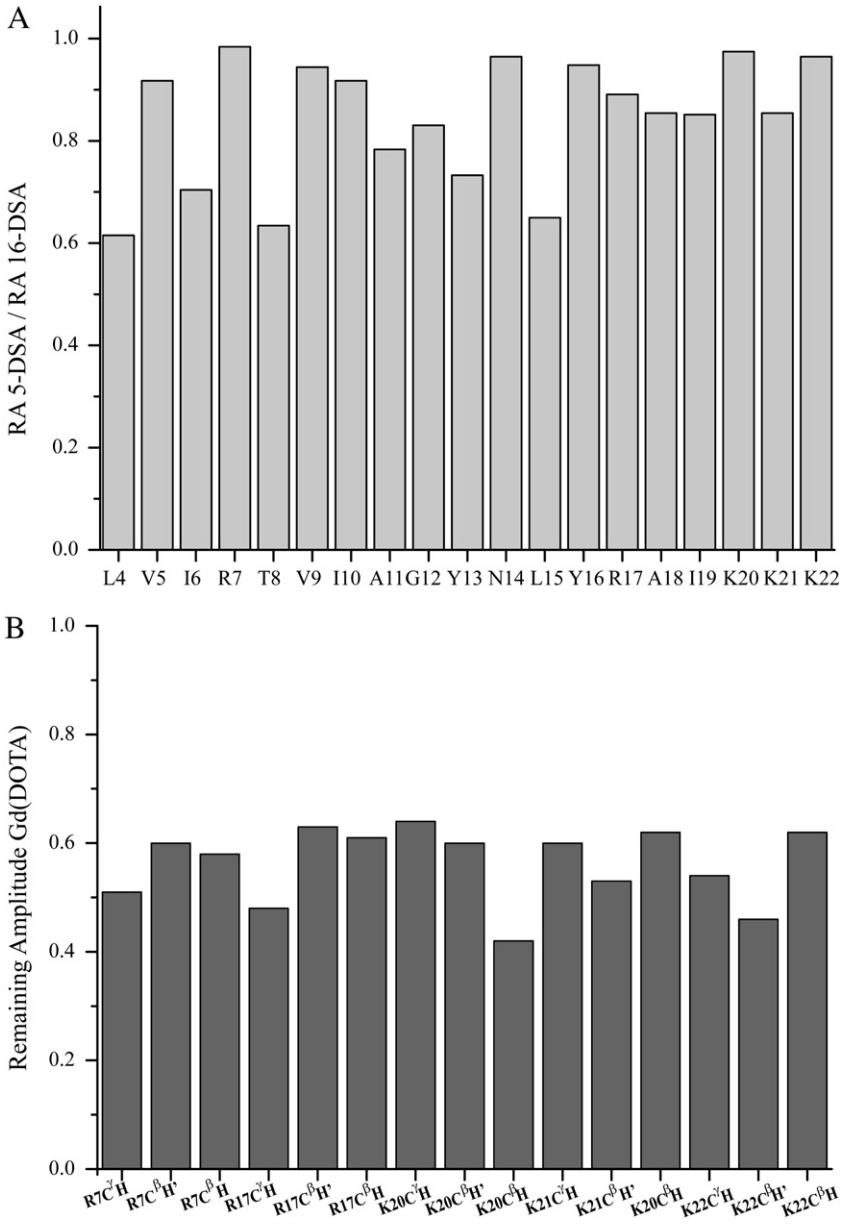

Fig. 7. Perturbation of NMR resonances of VK22 by spin labeled probes. (A) Bar diagram showing ratio of remaining signal amplitude upon additions of 5-DSA and 16-DSA. A ratio of 5-DSA/16-DSA ~1 is indicative of equal perturbation by both the spin labeled probes. A lower ratio value, <1.0, of 5-DSA/16-DSA indicates a higher perturbation by 5-DSA. Changes in intensity of intra-residue HN/C^{α}H cross-peaks in the NOESY spectra of VK22 were estimated before and after addition of 2 mM spin labeled doxyl lipids. (B) Bar diagram showing remaining amplitude of signal for sidechain resonances of cationic residues upon addition of soluble spin labeled quencher Gd^{3+}(DOTA). Gd^{3+}(DOTA) did not perturb backbone resonances of VK22 and therefore not shown.

exchange indicate that the central non-polar part of the tetrameric structure is located inside the hydrophobic core of the DPC micelles. It is, therefore, likely that the tetrameric structure of VK22 may be accommodated in the DPC micelles in an inserted or transmembrane mode of orientation. It is mention worthy that in a parallel orientation, one would expect a higher degree of resonance perturbation by Gd^{3+} (DOTA), as observed for AMPs attached to the surface of micelles [47,48]. The inserted orientation of VK22 tetramer could be sustained by charge complementarity whereby basic patches at the termini may reside at the phosphate head group regions of the micelles. The central hydrophobic segment of the tetramer acquires a position across the non-polar acyl chains of micelles (Fig. 4E). It is noteworthy that the head group to head group distance, 34 Å, of the DPC micelle [49] is compatible with the long axis length, 37 Å, of the tetramer (Fig. 4E).

3.6. Intrinsic tryptophan fluorescence

NMR studies have provided limited information for the first three residues, V–P–W segment, of VK22. In order to determine micelle localization of these residues Trp fluorescence and quenching experiments were carried out (Fig. 8A). Tryptophan residue of the free VK22 in aqueous buffer solution exhibits an emission maximum of 355 nm, characteristic of a solvent exposed fluorophore. In the presence of DPC micelles, a blue shift, ~335 nm, in the emission maxima of Trp has been observed, demonstrating incorporation of Trp residue into the hydrophobic environment of DPC micelles (Fig. 8A). Quenching of fluorescence intensity of DPC-bound VK22 with a water soluble neutral quencher acrylamide has been found to be restricted with a Stern–Volmer quenching constant (K_{sv}) of 8.6, the K_{sv} of free VK22 has been determined to be 26 (Fig. 8B). These results demonstrate that the N-terminal tri-peptide part, VWP, of VK22 is largely associated with the DPC micelles into its non-polar acyl region. As, Trp residue is often located at the hydrocarbon–water interfacial region in membrane proteins and peptides [50].

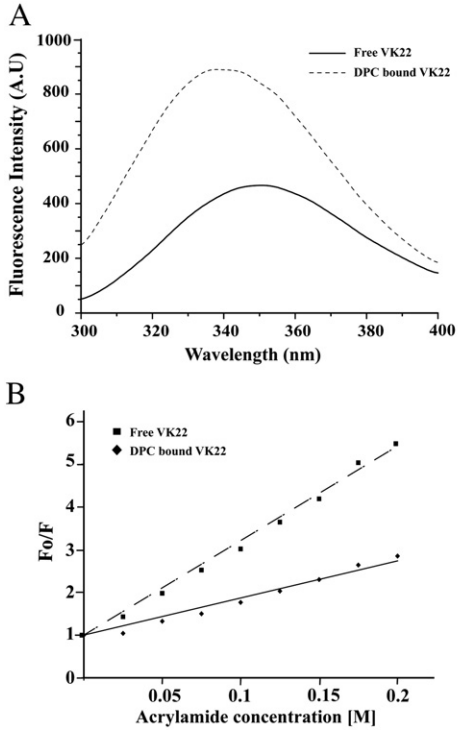

Fig. 8. Intrinsic Trp fluorescence studies of VK22. (A) Fluorescence emission spectra of VK22 without DPC micelles (solid line) and in presence of 1.5 mM DPC micelles (broken line). (B) Stern–Volmer plots showing quenching of Trp fluorescence intensity by acrylamide for free VK22 (broken line) and VK22 in DPC micelles (solid line). Fluorescence experiments were conducted with a peptide concentration of 5 μM dissolved in a 10-mM sodium phosphate buffer, pH 6.8. Samples were excited at 280 nm wavelength and emission was measured from 300 to 400 nm wavelength.

3.7. A plausible pore by tetrameric structure of VK22

Through the long axis of the tetrameric structure of VK22 clustering of Y13 and Y16 residues leaves limited space for any channel like passage (Fig. 5C). However, a slight reorganization of the sidechain of Tyr residues can "open" a small pore (Fig. 9A). Hypothetically, such displacement of sidechains may be induced by change in trans-membrane voltage or ion gradients. The pore can aid in passage of water and ions (Fig. 9B and C). However, a larger pore can indeed be formed by higher order oligomers (Fig. 9D). In the cross-linking experiments, population of such higher oligomeric states of VK22 has been detected (Fig. 1C).

4. Discussion

Oligomerization of host defense cationic AMPs has important consequences in their stability and broad spectrum of antimicrobial activities. Oligomerization of AMPs in physiological or free solutions may resist unwanted intracellular proteolytic degradation [51]. However, self-associations of AMPs in the context of lipid membranes may be directly related to the mechanism of actions e.g. toroidal pore, trans-membrane channel (barrel stave) or non-specific carpet mode [2,5,7–10]. Experiments with lipid vesicles had established association of AMPs from all major structural, α or β, classes [52–54]. Plausible oligomeric interfaces, relevant for pore formation in bacterial cell, have been deduced from x-ray structures of, well-folded in free solution, α and β defensins without lipid environments [55–57]. The crystal structure of HNP 3, an α-defensin, revealed a probable oligomerization interface in the amphipathic dimeric structure [55]. Vesicle leakage experiments demonstrated assembly of approximately six dimers of HNP forming an annular pore of 25 Å diameter [58]. An octameric multimer was deduced in the x-ray structure of human β-defensin 2 [56], whereas NMR studies detected dimerization of the human β-defensin 3 [59]. The oligomeric structures of β-defensins have been proposed to enhance net cationic surface charges causing efficient cell permeabilization [59]. A recent work, using solid state NMR method, had deduced a model of the oligomeric pore structure of protegrin-1, a disulphide bonded β-hairpin antimicrobial peptide, in lipid bilayers [60]. It appeared that the lateral association of four dimeric units of protegrin-1 forms an octameric water pore of 21 Å diameter [60].

By contrast to the folded, with or without lipids, β-sheet or β-hairpin AMPs, cationic host defense short helical AMPs acquire structure only upon binding to lipid vesicles or micelles. Therefore, determining oligomeric structure of helical AMPs is rather difficult as compared to β-sheet AMPs. Several biophysical studies had demonstrated oligomerization and pore formation of helical AMPs e.g. magainin, maculatin, citropin and aurein, in lipid bilayer [61–66]. Magainin, a well investigated antimicrobial peptide isolated from African clawed frog *Xenopus laevis*, demonstrated to exert its antibacterial activities through pore formation in membranes [61–65]. Studies have shown that there could be 4 to 6 magainin molecules creating a torodial pore in DMPC/DMPG lipid bilayer [61–63]. In the pore, oligomeric assembly of magainin proposed to assume a trans-bilayer orientation as opposed to surface bound parallel orientation [67,68]. The synergistic interactions between PGLa and magainin are manifested by pore formation whereby the PGLa/magainin hetero-dimer olgomerizes and inserted into lipid bilayers with a perpendicular orientation [67,68]. A dimeric structure of magainin was solved in DPPC vesicles using tr-NOESY method [69]. The magainin dimer assumes an anti-parallel orientation stabilized by packing between aromatic residues [69]. A highly potent analog of magainin called MSI-78 has been found to acquire a similar

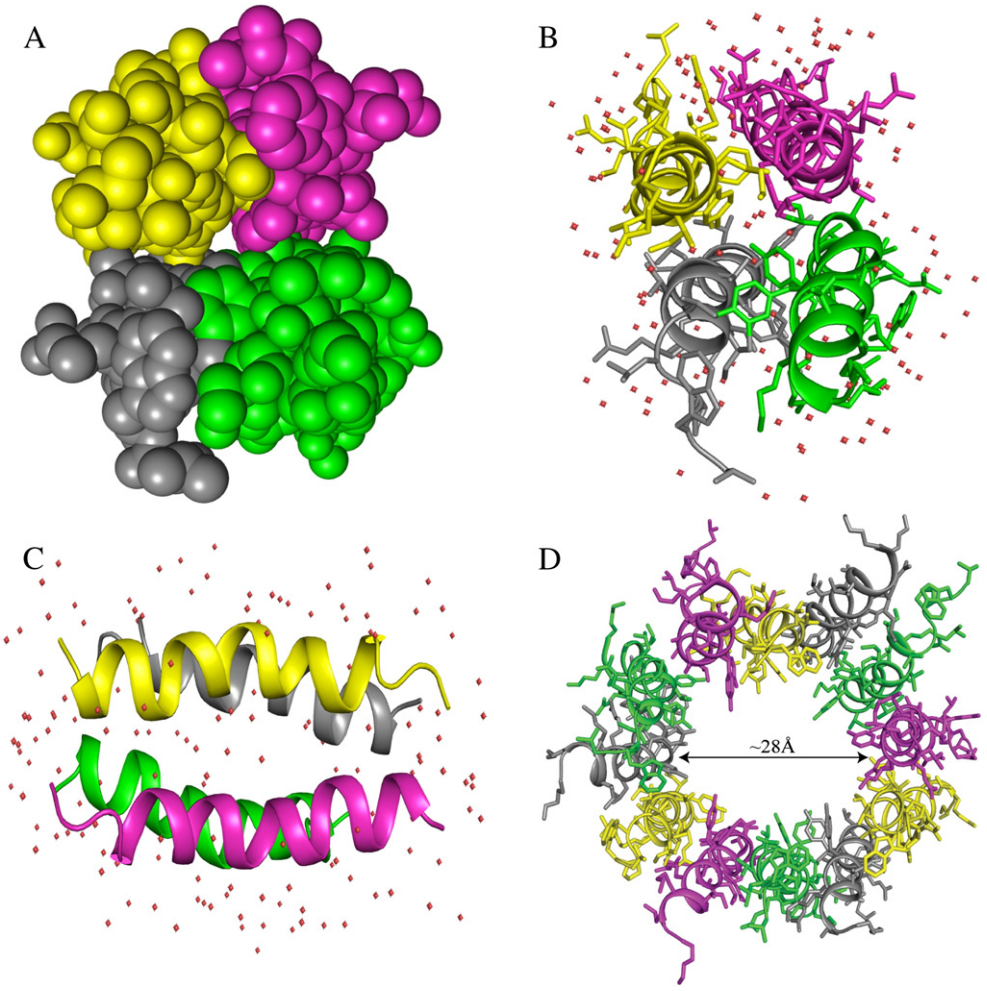

Fig. 9. Pore structure of VK22 tetramer. (A) A space-filling representation of the tetrameric structure, viewing down the helix axis, of VK22 showing location of the pore. (B and C) Water accessibility of the pore in the tetrameric structure of VK22 determined using the program SOAK (INSIGHT II). Water molecules are represented as red dots. (D) A representative structure of a potential dodecamer of VK22, determined using the same long range NOEs as in tetramer. The central pore size of the oligomer is indicated.

dimeric structure in DPC micelles [21]. Further, LL37, the human cathelicidin akin to fowlicidins, forms aggregated states in lipid environments [14]. While solid state NMR and spectroscopic methods delineated dimer formation or higher order oligomerization in lipid bilayer, monomeric helical structures of LL37 were obtained in DPC and SDS micelles [70,71].

Despite several compelling evidences suggesting oligomerizations of AMPs in lipid membranes are vital for their mode of actions; atomic resolution structures of AMPs in the oligomeric states in lipid membranes are scarce. In this work, we took the advantage of formation of tetrameric state of VK22 peptide in DPC micelles that has permitted us determination of atomic resolution structure of the oligomeric assembly. The NMR-derived structure of VK22 demonstrates primarily helical conformations, encompassing residues L4-K21, of the molecule in micelles. A considerable number of inter-peptide NOEs could be unambiguously detected due to the anti-parallel arrangements of the helices. Based on these NOEs, tetrameric structures of VK22 are obtained showing anti-parallel topology of four helices (Fig. 4). The helical bundle appears to be stabilized by mutual interactions among the four subunits by a number of hydrogen bonds and by non-polar packing interactions (Fig. 5). Noticeably, $T^{8}VIAG^{12}$ sequence motif of fowlicidin-1 shows multiple hydrogen bond contacts zipping two helical subunits of the DPC bound structure of VK22 (Fig. 5A). The micelle-bound structure of VK22 is further characterized by packing of Tyr residues at the helical interface (Fig. 5C). The tetrameric conformation of VK22 in DPC micelles essentially identifies two oligomerizing interfaces in the helical structure (Fig. 5A and B). As a matter of fact, higher oligomeric assemblies can be realized utilizing these interfaces to form even larger pores (Fig. 9C). Such pores are likely to be generated in the context of lipid bilayers or in cellular membranes. It may be noted that a monomeric NMR derived structure of fowlicidin-1 has been determined in aqueous tri-fluoro-ethanol (TFE) solution, as a membrane mimetic solvent [34]. In TFE, the N-terminal half of fowlicidin-1, residues R1-P7, did not adopt any regular conformations, whereas a helical structure was evident for the residues L8-K26 [34]. Therefore, membrane mimetic solvents like TFE might not be suitable to detect oligomerization of AMPs. Indeed, TFE and other fluoro-alcohols have been known to disrupt sidechain–sidechain interactions in soluble proteins [72,73]. It may be intriguing to observe a tetrameric form of VK22 in DPC micelles. Since, AMPs predominantly show monomeric structures in lipid micelles. The amino acid sequence of VK22 is distinctive whereby all the cationic residues are placed at the termini with the central segment is largely non-polar. This particular sequence characteristic could be playing an important role, along with other structural features, in the stabilization of oligomeric structures in DPC micelles.

The DPC-bound structure of VK22 may explain mechanism(s) of cell lysis. The electrostatic surface of the tetramer delineates a hydrophobic central region and cationic patches at the termini (Fig. 4E). We speculate that in a trans-membrane orientation, as appeared from spin labeled studies (Fig. 7), of the tetramer a barrel stave mode of action would be appropriate whereby the non-polar region at the middle of the oligomer resides along the acyl layer of the membrane and the positive charges at

the ends compliment phosphate head group interactions. The narrow pore along the helical interface will aid in permeation of ions and water molecules leading to the loss of osmotic balance and cell lysis (Fig. 9). Although a toroidal pore mechanism for VK22 may not be completely ruled out in the context of lipid bilayers. The large positively charged clusters of the oligomeric structure, interacting through phosphate head groups, can produce curvature or strains in the lipid bilayers. Such binding is implicated in closing the inner and outer leaflets of the bilayers [7–10]. The oligomeric structures may form the pore while lipid molecules align surrounding the pore structures. However, these mechanistic conjectures should be validated by further studies using model lipid bilayer systems. The atomic resolution structure of VK22 peptide can be further probed to understand correlations between peptide oligomerization with antimicrobial activities. In this study, we have shown a correlation plausibly exist, as replacement of Tyr to Ala showed lack of oligomerization and reduced antibacterial activities of VK22AA analog. Moreover, short membrane active peptides that undergo self-assembly into a definite quaternary structure in lipid environments might provide important scaffold for the design of membrane proteins [74,75]. Therefore, we envision that the tetrameric structure of VK22 will be further utilized for the generation of synthetic trans-membrane protein mimics with novel functions. In conclusion, we have determined a tetrameric structure of a potent, salt resistance antimicrobial peptide in detergent DPC micelles. The molecular interactions and lipid localization of the oligomeric structure will aid in the development of new antibiotics against drug resistant pathogens.

Acknowledgments

The work is supported in part by research grants 06/1/22/19/446, and 08/1/22/19/556 from A*BMRC, Singapore. RS is a recipient of a graduate fellowship from Nanyang Technological University. The atomic coordinates and NMR constrains of VK22 structure are deposited to BioMagResBank (BMRB) under the accession code 20125.

Appendix A. Supplementary data

Supplementary data to this article can be found online at doi:10.1016/j.bbamem.2010.10.001.

References

[1] M. Zasloff, Antimicrobial peptides of multicellular organisms, Nature 415 (2002) 389–395.
[2] K.A. Brogden, Antimicrobial peptides: pore formers or metabolic inhibitors in bacteria? Nat. Rev. Microbiol. 3 (2005) 238–250.
[3] R.E. Hancock, M.G. Scott, The role of antimicrobial peptides in animal defenses, Proc. Natl Acad. Sci. USA 97 (2000) 8856–8861.
[4] H.G. Boman, Peptide antibiotics and their role in innate immunity, Annu. Rev. Immunol. 13 (1995) 61–92.
[5] Z. Oren, Y. Shai, Mode of action of linear amphipathic alpha-helical antimicrobial peptides, Biopolymers 47 (1998) 451–463.
[6] H.W. Huang, Action of antimicrobial peptides: two-state model, Biochemistry 39 (2000) 8347–8352.
[7] K. Matsuzaki, Magainins as paradigm for the mode of action of pore forming polypeptides, Biochim. Biophys. Acta 1376 (1998) 391–400.
[8] R.M. Epand, H.J. Vogel, Diversity of antimicrobial peptides and their mechanisms of action, Biochim. Biophys. Acta 1462 (1999) 11–28.
[9] B. Bechinger, The structure, dynamics and orientation of antimicrobial peptides in membranes by multidimensional solid-state NMR spectroscopy, Biochim. Biophys. Acta 1462 (1999) 157–183.
[10] Y. Shai, Mechanism of the binding, insertion and destabilization of phospholipid bilayer membranes by alpha-helical antimicrobial and cell non-selective membrane-lytic peptides, Biochim. Biophys. Acta 1462 (1999) 55–70.
[11] E.F. Haney, H.N. Hunter, K. Matsuzaki, H.J. Vogel, Solution NMR studies of amphibian antimicrobial peptides: linking structure to function? Biochim. Biophys. Acta 1788 (2009) 1639–1655.
[12] A. Ramamoorthy, Beyond NMR spectra of antimicrobial peptides: dynamical images at atomic resolution and functional insights, Solid State Nucl. Magn. Reson. 35 (2009) 201–207.
[13] M. Hong, Solid-state NMR studies of the structure, dynamics, and assembly of beta-sheet membrane peptides and alpha-helical membrane proteins with antibiotic activities, Acc. Chem. Res. 39 (2006) 176–183.
[14] A. Ramamoorthy, D.K. Lee, J.S. Santos, K.A. Henzler-Wildman, Nitrogen-14 solid-state NMR spectroscopy of aligned phospholipid bilayers to probe peptide-lipid interaction and oligomerization of membrane associated peptides, J. Am. Chem. Soc. 130 (2008) 11023–11029.
[15] S. Afonin, S.L. Grage, M. Ieronimo, P. Wadhwani, A.S. Ulrich, Temperature-dependent transmembrane insertion of the amphiphilic peptide PGLa in lipid bilayers observed by solid state 19F NMR spectroscopy, J. Am. Chem. Soc. 130 (2008) 16512–16514.
[16] D.I. Chan, E.J. Prenner, H.J. Vogel, Tryptophan- and arginine-rich antimicrobial peptides: structures and mechanisms of action, Biochim. Biophys. Acta 1758 (2006) 1184–1202.
[17] S.K. Straus, R.E. Hancock, Mode of action of the new antibiotic for Gram-positive pathogens daptomycin: comparison with cationic antimicrobial peptides and lipopeptides, Biochim. Biophys. Acta 1758 (2006) 1215–1223.
[18] J.P. Powers, A. Tan, A. Ramamoorthy, R.E. Hancock, Solution structure and interaction of the antimicrobial polyphemusins with lipid membranes, Biochemistry 44 (2005) 15504–15513.
[19] P. Rogne, G. Fimland, J. Nissen-Meyer, P.E. Kristiansen, Three-dimensional structure of the two peptides that constitute the two-peptide bacteriocin lactococcin G, Biochim. Biophys. Acta 1784 (2008) 543–554.
[20] G. Wang, Determination of solution structure and lipid micelle location of an engineered membrane peptide by using one NMR experiment and one sample, Biochim. Biophys. Acta 1768 (2007) 3271–3281.
[21] F. Porcelli, B.A. Buck-Koehntop, S. Thennarasu, A. Ramamoorthy, G. Veglia, Structures of the dimeric and monomeric variants of magainin antimicrobial peptides (MSI-78 and MSI-594) in micelles and bilayers, determined by NMR spectroscopy, Biochemistry 45 (2006) 5793–5799.
[22] C. Roumestand, V. Louis, A. Aumelas, G. Grassy, B. Calas, A. Chavanieu, Oligomerization of protegrin-1 in the presence of DPC micelles. A proton high-resolution NMR study, FEBS Lett. 421 (1998) 263–267.
[23] T.V. Ovchinnikova, Z.O. Shenkarev, S.V. Balandin, K.D. Nadezhdin, A.S. Paramonov, V.N. Kokryakov, A.S. Arseniev, Molecular insight into mechanism of antimicrobial action of the beta-hairpin peptide arenicin: specific oligomerization in detergent micelles, Biopolymers 89 (2008) 455–464.
[24] R.T. Syvitski, I. Burton, N.R. Mattatall, S.E. Douglas, D.L. Jakeman, Structural characterization of the antimicrobial peptide pleurocidin from winter flounder, Biochemistry 44 (2005) 7282–7293.
[25] S. Hiller, G. Wagner, The role of solution NMR in the structure determinations of VDAC-1 and other membrane proteins, Curr. Opin. Struct. Biol. 19 (2009) 396–401.
[26] A. Arora, L.K. Tamm, Biophysical approaches to membrane protein structure determination, Curr. Opin. Struct. Biol. 11 (2001) 540–547.
[27] J. Zamoon, F. Nitu, C. Karim, D.D. Thomas, G. Veglia, Mapping the interaction surface of a membrane protein: unveiling the conformational switch of phospholamban in calcium pump regulation, Proc. Natl Acad. Sci. USA 102 (2005) 4747–4752.
[28] S. Bhattacharjya, A. Ramamoorthy, Multifunctional host defense peptides: functional and mechanistic insights from NMR structures of potent antimicrobial peptides, FEBS J. 276 (2009) 6465–6473.
[29] A. Bhunia, H. Mohanram, P.N. Domadia, J. Torres, S. Bhattacharjya, Designed beta-boomerang antiendotoxic and antimicrobial peptides: structures and activities in lipopolysaccharide, J. Biol. Chem. 284 (2009) 21991–22004.
[30] U.H. Durr, U.S. Sudheendra, A. Ramamoorthy, LL-37, the only human member of the cathelicidin family of antimicrobial peptides, Biochim. Biophys. Acta 1758 (2006) 1408–1425.
[31] R. Gennaro, M. Zanetti, Structural features and biological activities of the cathelicidin-derived antimicrobial peptides, Biopolymers 55 (2000) 31–49.
[32] A. Bardan, V. Nizet, R.L. Gallo, Antimicrobial peptides and the skin, Expert Opin. Biol. Ther. 4 (2004) 543–549.
[33] Y. Xiao, Y. Cai, Y.R. Bommineni, S.C. Fernando, O. Prakash, S.E. Gilliland, G. Zhang, Identification and functional characterization of three chicken cathelicidins with potent antimicrobial activity, J. Biol. Chem. 281 (2006) 2858–2867.
[34] Y. Xiao, H. Dai, Y.R. Bommineni, J.L. Soulages, Y.X. Gong, O. Prakash, G. Zhang, Structure-activity relationships of fowlicidin-1, a cathelicidin antimicrobial peptide in chicken, FEBS J. 273 (2006) 2581–2593.
[35] Y.R. Bommineni, H. Dai, Y.X. Gong, J.L. Soulages, S.C. Fernando, U. Desilva, O. Prakash, G. Zhang, Fowlicidin-3 is an alpha-helical cationic host defense peptide with potent antibacterial and lipopolysaccharide-neutralizing activities, FEBS J. 274 (2007) 418–428.
[36] K Wuthrich, NMR of proteins and nucleic acids (1986).
[37] R. Saravanan, A. Bhunia, S. Bhattacharjya, Micelle-bound structures and dynamics of the hinge deleted analog of melittin and its diastereomer: implications in cell selective lysis by D-amino acid containing antimicrobial peptides, Biochim. Biophys. Acta 1798 (2010) 128–139.
[38] G. Cornilescu, F. Delaglio, A. Bax, Protein backbone angle restraints from searching a database for chemical shift and sequence homology, J. Biomol. NMR 13 (1999) 289–302.
[39] P. Guntert, C. Mumenthaler, K. Wuthrich, Torsion angle dynamics for NMR structure calculation with the new program DYANA, J. Mol. Biol. 273 (1997) 283–298.
[40] Y. Rosenfeld, N. Papo, Y. Shai, Endotoxin (lipopolysaccharide) neutralization by innate immunity host-defense peptides. Peptide properties and plausible modes of action, J. Biol. Chem. 281 (2006) 1636–1643.
[41] D.P.H.A.S. Altieri, R.A. Byrd, Association of biomolecular systems via pulsed field gradient NMR self-diffusion measurements, J. Am. Chem. Soc. 117 (1995) 7561–7566.

[42] D.S. Wishart, B.D. Sykes, F.M. Richards, The chemical shift index: a fast and simple method for the assignment of protein secondary structure through NMR spectroscopy, Biochemistry 31 (1992) 1647–1651.
[43] A. Senes, I. Ubarretxena-Belandia, D.M. Engelman, The Calpha--H...O hydrogen bond: a determinant of stability and specificity in transmembrane helix interactions, Proc. Natl Acad. Sci. USA 98 (2001) 9056–9061.
[44] A. Senes, M. Gerstein, D.M. Engelman, Statistical analysis of amino acid patterns in transmembrane helices: the GxxxG motif occurs frequently and in association with beta-branched residues at neighboring positions, J. Mol. Biol. 296 (2000) 921–936.
[45] R.F. Walters, W.F. DeGrado, Helix-packing motifs in membrane proteins, Proc. Natl Acad. Sci. USA 103 (2006) 13658–13663.
[46] C. Hilty, G. Wider, C. Fernandez, K. Wuthrich, Membrane protein-lipid interactions in mixed micelles studied by NMR spectroscopy with the use of paramagnetic reagents, Chembiochem 5 (2004) 467–473.
[47] Z.O. Shenkarev, K.D. Nadezhdin, V.A. Sobol, A.G. Sobol, L. Skjeldal, A.S. Arseniev, Conformation and mode of membrane interaction in cyclotides. Spatial structure of kalata B1 bound to a dodecylphosphocholine micelle, FEBS J. 273 (2006) 2658–2672.
[48] M. Respondek, T. Madl, C. Gobl, R. Golser, K. Zangger, Mapping the orientation of helices in micelle-bound peptides by paramagnetic relaxation waves, J. Am. Chem. Soc. 129 (2007) 5228–5234.
[49] L. Columbus, J. Lipfert, K. Jambunathan, D.A. Fox, A.Y. Sim, S. Doniach, S.A. Lesley, Mixing and matching detergents for membrane protein NMR structure determination, J. Am. Chem. Soc. 131 (2009) 7320–7326.
[50] M. de Planque, B.B. Bonev, J.A. Demmers, D.V. Greathouse, R.E. Koeppe II, F. Separovic, A. Watts, J.A. Killian, Interfacial anchor properties of tryptophan residues in transmembrane peptides can dominate over hydrophobic matching effects in peptide–lipid interactions, Biochemistry 42 (2003) 5341–5348.
[51] D. Raimondo, G. Andreotti, N. Saint, P. Amodeo, G. Renzone, M. Sanseverino, I. Zocchi, G. Molle, A. Motta, A. Scaloni, A folding-dependent mechanism of antimicrobial peptide resistance to degradation unveiled by solution structure of distinctin, Proc. Natl Acad. Sci. USA 102 (2005) 6309–6314.
[52] K. Matsuzaki, O. Murase, N. Fujii, K. Miyajima, An antimicrobial peptide, magainin 2, induced rapid flip-flop of phospholipids coupled with pore formation and peptide translocation, Biochemistry 35 (1996) 11361–11368.
[53] M.T. Lee, W.C. Hung, F.Y. Chen, H.W. Huang, Mechanism and kinetics of pore formation in membranes by water-soluble amphipathic peptides, Proc. Natl Acad. Sci. USA 105 (2008) 5087–5092.
[54] K. He, S.J. Ludtke, H.W. Huang, D.L. Worcester, Antimicrobial peptide pores in membranes detected by neutron in-plane scattering, Biochemistry 34 (1995) 15614–15618.
[55] C.P. Hill, J. Yee, M.E. Selsted, D. Eisenberg, Crystal structure of defensin HNP-3, an amphiphilic dimer: mechanisms of membrane permeabilization, Science 251 (1991) 1481–1485.
[56] D.M. Hoover, K.R. Rajashankar, R. Blumenthal, A. Puri, J.J. Oppenheim, O. Chertov, J. Lubkowski, The structure of human beta-defensin-2 shows evidence of higher order oligomerization, J. Biol. Chem. 275 (2000) 32911–32918.
[57] A. Szyk, Z. Wu, K. Tucker, D. Yang, W. Lu, J. Lubkowski, Crystal structures of human alpha-defensins HNP4, HD5, and HD6, Protein Sci. 15 (2006) 2749–2760.
[58] W.C. Wimley, M.E. Selsted, S.H. White, Interactions between human defensins and lipid bilayers: evidence for formation of multimeric pores, Protein Sci. 3 (1994) 1362–1373.
[59] D.J. Schibli, H.N. Hunter, V. Aseyev, T.D. Starner, J.M. Wiencek, P.B. McCray Jr., B.F. Tack, H.J. Vogel, The solution structures of the human beta-defensins lead to a better understanding of the potent bactericidal activity of HBD3 against *Staphylococcus aureus*, J. Biol. Chem. 277 (2002) 8279–8289.
[60] R. Mani, S.D. Cady, M. Tang, A.J. Waring, R.I. Lehrer, M. Hong, Membrane-dependent oligomeric structure and pore formation of a beta-hairpin antimicrobial peptide in lipid bilayers from solid-state NMR, Proc. Natl Acad. Sci. USA 103 (2006) 16242–16247.
[61] S.J. Ludtke, K. He, W.T. Heller, T.A. Harroun, L. Yang, H.W. Huang, Membrane pores induced by magainin, Biochemistry 35 (1996) 13723–13728.
[62] L. Yang, T.A. Harroun, W.T. Heller, T.M. Weiss, H.W. Huang, Neutron off-plane scattering of aligned membranes. I. Method of measurement, Biophys. J. 75 (1998) 641–645.
[63] K. Matsuzaki, O. Murase, H. Tokuda, S. Funakoshi, N. Fujii, K. Miyajima, Orientational and aggregational states of magainin 2 in phospholipid bilayers, Biochemistry 33 (1994) 3342–3349.
[64] K. Matsuzaki, Magainins as paradigm for the mode of action of pore forming polypeptides, Biochim. Biophys. Acta 1376 (1998) 391–400.
[65] T. Hara, H. Kodama, M. Kondo, K. Wakamatsu, A. Takeda, T. Tachi, K. Matsuzaki, Effects of peptide dimerization on pore formation: antiparallel disulfide-dimerized magainin 2 analogue, Biopolymers 58 (2001) 437–446.
[66] E.E. Ambroggio, F. Separovic, J.H. Bowie, G.D. Fidelio, L.A. Bagatolli, Direct visualization of membrane leakage induced by the antibiotic peptides: maculatin, citropin, and aurein, Biophys. J. 89 (2005) 1874–1881.
[67] E. Strandberg, P. Tremouilhac, P. Wadhwani, A.S. Ulrich, Synergistic transmembrane insertion of the heterodimeric PGLa/magainin 2 complex studied by solid-state NMR, Biochim. Biophys. Acta 1788 (2009) 1667–1679.
[68] P. Tremouilhac, E. Strandberg, P. Wadhwani, A.S. Ulrich, Synergistic transmembrane alignment of the antimicrobial heterodimer PGLa/magainin, J. Biol. Chem. 281 (2006) 32089–32094.
[69] K. Wakamatsu, A. Takeda, T. Tachi, K. Matsuzaki, Dimer structure of magainin 2 bound to phospholipid vesicles, Biopolymers 64 (2002) 314–327.
[70] F. Porcelli, R. Verardi, L. Shi, K.A. Henzler-Wildman, A. Ramamoorthy, G. Veglia, NMR structure of the cathelicidin-derived human antimicrobial peptide LL-37 in dodecylphosphocholine micelles, Biochemistry 47 (2008) 5565–5572.
[71] G. Wang, Structures of human host defense cathelicidin LL-37 and its smallest antimicrobial peptide KR-12 in lipid micelles, J. Biol. Chem. 283 (2008) 32637–32643.
[72] M. Buck, Trifluoroethanol and colleagues: cosolvents come of age. Recent studies with peptides and proteins, Q Rev. Biophys. 31 (1998) 297–355.
[73] S. Bhattacharjya, P. Balaram, Hexafluoroacetone hydrate as a structure modifier in proteins: characterization of a molten globule state of hen egg-white lysozyme, Protein Sci. 6 (1997) 1065–1073.
[74] H. Yin, J.S. Slusky, B.W. Berger, R.S. Walters, G. Vilaire, R.I. Litvinov, J.D. Lear, G.A. Caputo, J.S. Bennett, W.F. DeGrado, Computational design of peptides that target transmembrane helices, Science 315 (2007) 1817–1822.
[75] W.F. DeGrado, H. Gratkowski, J.D. Lear, How do helix–helix interactions help determine the folds of membrane proteins? Perspectives from the study of homo-oligomeric helical bundles, Protein Sci. 12 (2003) 647–665.